Device

Article

From nature's deadly strike to safety protection: Mantis shrimp-inspired ultrafast energy transformation for smart surveillance

Graphical abstract

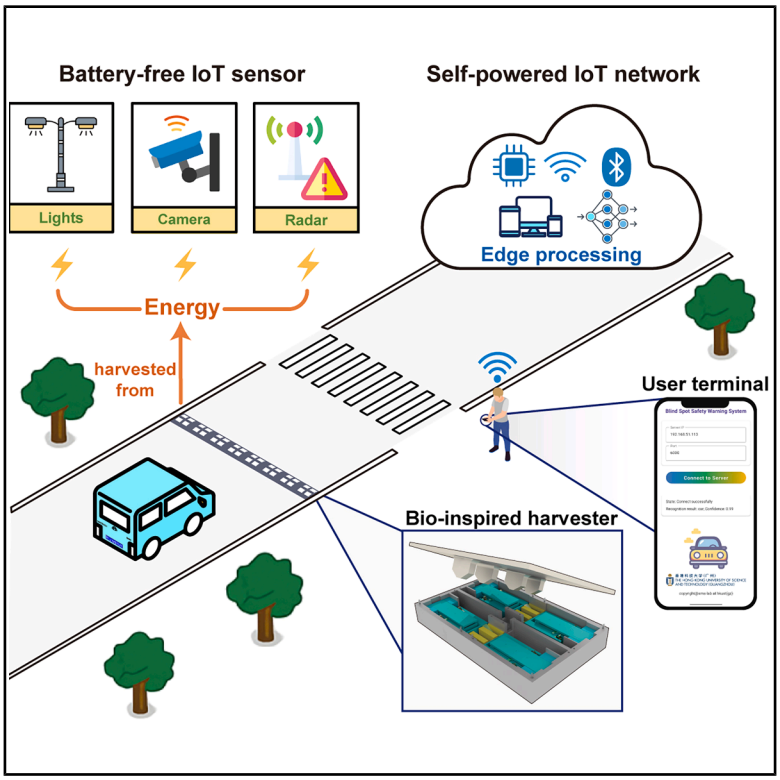

Highlights

- A bio-inspired energy harvester mimics the mantis shrimp's strike mechanism
- Achieves a record-high 1,867 W/m^3 power density via latch-mediated energy conversion
- Powers radar/camera modules solely with energy harvested from vehicle motion
- Potential to advance scalable, self-powered intelligent transportation infrastructure

Authors

Yihao Li, Yizhou Li, Yawei Wang, ..., Xin Li, Wei-Hsin Liao, Guobiao Hu

Correspondence

xinli001@cuhk.edu.hk (X.L.), guobiaohu@hkust-gz.edu.cn (G.H.)

In brief

This work presents a bio-inspired energy harvester that mimics the mantis shrimp's ultrafast strike mechanism, enabling consistent energy output independent of excitation frequency or speed. The system reliably captures kinetic energy from footsteps or passing vehicles, supporting a wide range of self-powered IoT applications. Demonstrated in transportation scenarios, it powers radar and image capture modules for hazard detection without batteries. By integrating biomechanics with sustainable energy technology, this work offers a scalable solution for battery-free surveillance and next-generation smart infrastructure.

Develop
Prototype with demonstrated applications in relevant environment

Li et al., 2025, Device *3*, 100903
November 21, 2025
Published by Elsevier Inc.
https://doi.org/10.1016/j.device.2025.100903

CellPress

Please cite this article in press as: Li et al., From nature's deadly strike to safety protection: Mantis shrimp-inspired ultrafast energy transformation for smart surveillance, Device (2025), https://doi.org/10.1016/j.device.2025.100903

Device

CellPress
OPEN ACCESS

Article

From nature's deadly strike to safety protection: Mantis shrimp-inspired ultrafast energy transformation for smart surveillance

Yihao Li,[1,5] Yizhou Li,[1,5] Yawei Wang,[1,5] Mianxin Xiao,[2,5] Hao Tang,[1] Yunlong Zi,[3] Junlei Wang,[4] Xin Li,[2,*] Wei-Hsin Liao,[2] and Guobiao Hu[1,6,*]

[1]Thrust of Internet of Things, The Hong Kong University of Science and Technology (Guangzhou), Nansha, Guangzhou, Guangdong 511400, China

[2]Department of Mechanical and Automation Engineering, The Chinese University of Hong Kong, Shatin, NT, Hong Kong 999077, China

[3]Thrust of Sustainable Energy and Environment, The Hong Kong University of Science and Technology (Guangzhou), Nansha, Guangzhou, Guangdong 511400, China

[4]School of Mechanical and Power Engineering, Zhengzhou University, Zhengzhou 450000, China

[5]These authors contributed equally

[6]Lead contact

*Correspondence: xinli001@cuhk.edu.hk (X.L.), guobiaohu@hkust-gz.edu.cn (G.H.)

https://doi.org/10.1016/j.device.2025.100903

THE BIGGER PICTURE The quest for sustainable power solutions drives innovation in bio-inspired energy harvesting. This study transcends conventional biomimicry by enhancing nature's design—transforming the mantis shrimp's strike mechanism into a carefully engineered system that employs latch-mediated energy conversion and overcomes biological limitations. Beyond generating record-high power density, the system seamlessly integrates kinetic energy harvesting with ubiquitous Internet of Things (IoT), enabling battery-free sensing and communication at the edge. Such bio-inspired engineering could fundamentally revolutionize IoT networks by enabling self-powered operation through converting commonplace mechanical motions, such as human footsteps and vehicle-induced vibrations, into reliable energy sources applicable across diverse domains. By uniting biomechanics, electromagnetic transduction, and deep learning, this work has outlined a scalable and maintenance-free framework for next-generation monitoring systems in transportation and security infrastructure.

SUMMARY

Inspired by the ultrafast strike of the mantis shrimp, we present an energy harvester (mantis shrimp-inspired energy harvester [MSEH]) that employs an enhanced latch-mediated spring actuation (LaMSA) mechanism, functionally surpassing its biological counterpart, to enable highly efficient mechanical-to-electrical energy conversion. The MSEH delivers a peak voltage of 60 V and a maximum instantaneous power of 7.74 W, yielding up to 44.24 mJ per trigger and exceeding the power density of most existing electromagnetic energy harvesters. Field tests confirm that four MSEH units integrated into a compact power-generating floor can collectively produce approximately 180 mJ, subjected to a single trigger, sufficient to power an ultra-low-power radar or image-sensing module for Internet of Things (IoT) applications. The radar enables real-time vehicle proximity detection, while the camera captures and transmits images to a ConvNeXt model for object recognition. These findings underscore the MSEH's exceptional power density (1,867.41 W/m^3), reliable energy output, and potential to support scalable, self-powered intelligent systems.

INTRODUCTION

Predators in nature have evolved a variety of astonishing mechanisms, and one of the most remarkable examples is the deadly strike of the mantis shrimp.[1–4] This small but powerful creature can deliver one of the fastest and most forceful strikes in the animal kingdom with an acceleration reaching 10^6 rad/s^2 in water.[5] The impact is so extreme that it can even generate cavitation bubbles,[6] a phenomenon where the strike creates vapor-filled cavities that collapse with immense energy, producing secondary shockwaves. Unlike artificial technologies, such as torpedoes or super-cavitating submarines, mantis shrimps achieve

Please cite this article in press as: Li et al., From nature's deadly strike to safety protection: Mantis shrimp-inspired ultrafast energy transformation for smart surveillance, Device (2025), https://doi.org/10.1016/j.device.2025.100903

this effect effortlessly despite their centimeter-scale body size. This highlights the exceptional efficiency of the mantis shrimp in energy utilization and transformation. Its extraordinary evolutionary adaptation has inspired innovative bioengineered designs.[7] While the biomechanics of the mantis shrimp have been extensively studied[8–13] and researchers have developed mechanical systems to replicate its formidable strike,[5,14–16] the profound potential of its highly efficient energy transformation mechanism remains largely unexplored, with little effort devoted to harnessing it for practical applications. Unlocking this bio-inspired energy conversion mechanism could lead to groundbreaking advancements in fields such as energy harvesting, impact mitigation, and high-speed actuation systems.

Bio-inspired energy conversion and harvesting have garnered increasing attention[17–21] as researchers strive to develop efficient and sustainable methods for collecting energy from the ambient environment. Many insects and certain animals with specialized biomechanics exhibit remarkable energy conversion mechanisms, such as latch-mediated spring actuation (LaMSA)[13,22] and muscle-spring power modulation,[23] that enable gradual storage and rapid release of energy to generate high-speed movements. These biological principles have inspired the development of engineered systems that embed elastic energy storage within their structures, exemplified by robotic manipulators featuring spring-latch modules[15] and soft robots capable of insect-like jumping.[24] By embedding energy storage into robotics, they envisioned the potential for efficient and multifunctional energy utilization.[25] In addition, triboelectric and/or piezoelectric nanogenerators have been inspired by the locomotion of animals, such as human walking and fish swimming, to harvest mechanical energy from kinetic motion.[26–28] Meanwhile, bioelectric energy harvesters have been developed based on the ion exchange mechanism of electric eels, enabling artificial power generation through electrolyte transport.[29–31]

Despite these advancements, most bio-inspired energy generators and harvesters primarily mimic form, motion, or structural efficiency rather than fully exploiting biomechanical energy transformation. Moreover, they remain largely underdeveloped, with limited power generation capacity, rendering them impractical for real-world applications. The ultrafast biomechanical energy transformation discussed in this work, such as the mantis shrimp's deadly strike, remains largely untapped. This gap presents an opportunity to develop novel and high-power-density energy conversion systems that can harness motion for applications in self-powered electronics, intelligent monitoring, and autonomous systems.

Leveraging the biomechanics behind the mantis shrimp's deadly strike, as illustrated in Figure 1A, we translated its functional anatomy into a biomimetic framework. As shown in Figure 1B, the saddle acts as an elastic energy storage element, while the merus-carpus linkage and latch system work in coordination to regulate energy accumulation and rapid release. This biological actuation follows a three-phase sequence—energy input, storage, and release—conceptually illustrated in Figure 1C using an archery analogy. Drawing on these principles, we designed the mantis shrimp-inspired energy harvester (MSEH) with analogous components: buffer springs to store elastic energy; a dual-latch system, consisting of a self-locking latch and a button latch, to control the storage and release phases; and a magnet array that, upon release, moves at high speeds to induce an electromotive force via electromagnetic induction. The integration of these components into a compact mechanical system is shown in Figure 1E. It utilizes a latch-mediated energy storage/release mechanism, mimicking the mantis shrimp's spring-actuated appendage to achieve rapid energy transformation (Figures 1F–1I). It is worth mentioning that while many biological and bio-inspired systems are highly efficient, they are typically constrained to small sizes.[13] Scaling them up to larger dimensions while preserving their efficiency is challenging. This is exemplified by the fact that certain specialized biological mechanisms in insects (e.g., trap-jaw ants[32] and froghoppers[33]) exhibit remarkably higher efficiency, quantified in terms of power amplification,[34] than those in large mammals (e.g., cheetahs[35] and humans[36]). One significant breakthrough presented in this work is evident through the comparison in Table S8, where our proposed MSEH outperforms existing designs[32,34,37–41] by achieving a mass increase of several orders of magnitude while maintaining high efficiency. Beyond those biomimetic advantages, the MSEH also demonstrates superior performance compared to conventional energy harvesters. Figure 1D presents a comparison with representative examples from the literature,[42–49] where the MSEH is distinctly positioned in the top left corner—indicating a significantly higher power density than all other designs while retaining a relatively compact volume. By efficiently converting slow external forces into high-speed motion, then electricity, the MSEH is an ideal candidate for self-powered intelligent surveillance systems.

To explore the great potential of this MSEH and demonstrate its practical application, we integrate MSEH units into an autonomous intelligent monitoring system (Figure 1J), where the harvested energy powers a radar sensor and/or an ultra-low-power camera for motion-triggered safety alerts and notifications. We further integrate a deep learning model for object recognition based on the ConvNeXt architecture into the system, enabling precise differentiation between pedestrians and vehicles. The system's performance and functionality are thoroughly evaluated. Our results demonstrate that four MSEH units generate sufficient energy to power the radar or camera system, while deep-learning-model-based object recognition achieves high classification accuracy. This bio-inspired approach provides a scalable, efficient, and sustainable solution for motion-triggered, energy-autonomous surveillance, with promising applications in intelligent transportation, security monitoring, and smart urban infrastructure.

RESULTS AND DISCUSSION

Bio-inspired mechanism design

Figure 2A provides an overview of a mantis shrimp, highlighting the key anatomical features that enable its powerful strike. The inset illustrates that its appendage comprises three main components: a spring-loading mechanism, a rotating joint, and a latch system. In biomechanical terms, the spring-loading mechanism is an elastic exoskeleton that stores potential energy when compressed, while the latch system controls the release of this energy. When preparing to strike, the latch system is activated

Please cite this article in press as: Li et al., From nature's deadly strike to safety protection: Mantis shrimp-inspired ultrafast energy transformation for smart surveillance, Device (2025), https://doi.org/10.1016/j.device.2025.100903

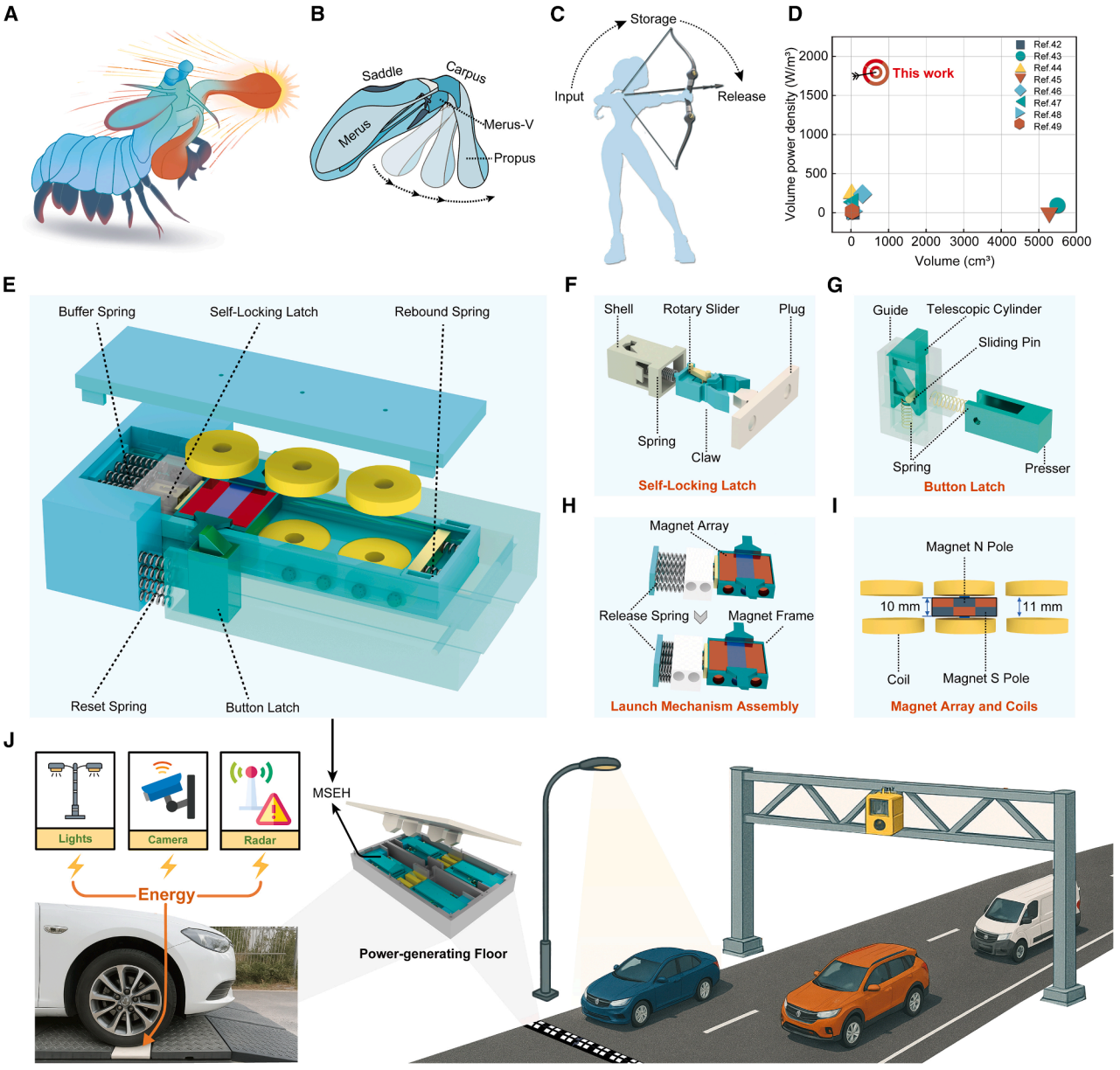

Figure 1. Overview of the mantis shrimp-inspired energy harvester and its application in energy-autonomous intelligent surveillance

(A) Illustration of a mantis shrimp executing its deadly strike.

(B) Bio-structure of a mantis shrimp's appendage.

(C) Conceptual analogy illustrating the energy storage and release mechanism behind a mantis shrimp's powerful strike, likened to archery: energy is first input and stored and then rapidly released.

(D) Comparison of the volume power density of the mantis shrimp-inspired energy harvester (MSEH) with existing designs, highlighting its superior performance.

(E) Exploded view of the MSEH, showing key components including the self-locking latch, button latch, buffer springs, magnets, and coils.

(F and G) Schematic of the self-locking latch and button latch switches, mimicking the shrimp's latch-mediated mechanism.

(H) The magnet-based launch mechanism assembly.

(I) The magnet array and coils for mechanical-to-electrical energy conversion.

(J) Integration of MSEH units into a power-generating floor for intelligent surveillance applications. The harvested energy powers low-power devices such as radars and cameras, enabling motion-triggered monitoring for smart transportation and security systems.

(latched/latch on) to hold the appendage in place and prevent it from rotating. At the same time, extensor muscles contract, storing energy in the spring-loading mechanism. Then, the latch system is released (unlatched/latch off). Upon release, the energy stored in the spring is rapidly converted into kinetic energy, propelling the shrimp's appendage with explosive force. The two

Please cite this article in press as: Li et al., From nature's deadly strike to safety protection: Mantis shrimp-inspired ultrafast energy transformation for smart surveillance, Device (2025), https://doi.org/10.1016/j.device.2025.100903

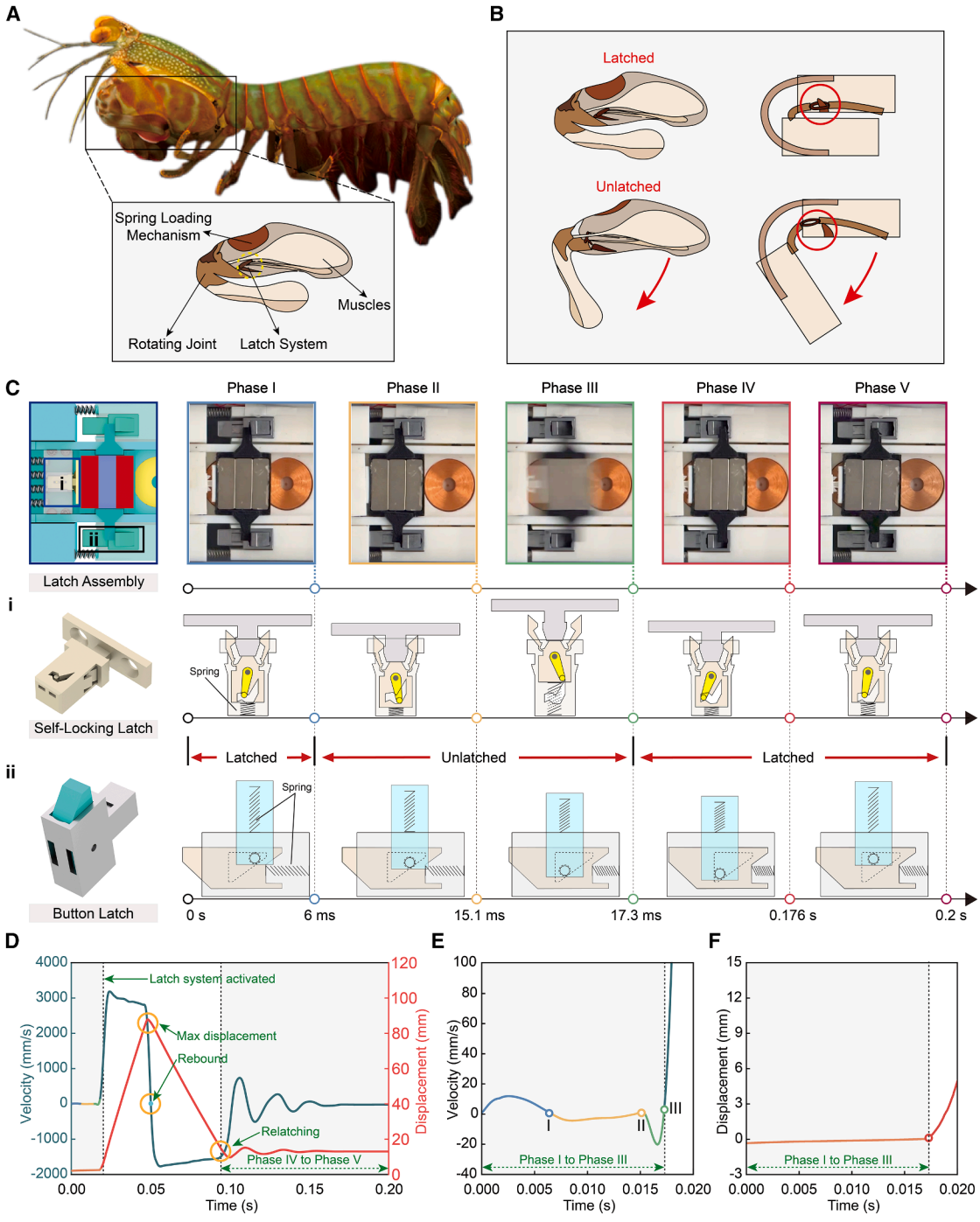

Figure 2. Mantis shrimp-inspired latch-mediated energy storage and release mechanism

(A) The biomechanical structure of a mantis shrimp's raptorial appendage, highlighting the spring-loading mechanism, rotating joint, muscles, and latch system responsible for its ultrafast strike. Image of mantis shrimp, copyright Joel Sartore/Photo Ark.

(B) Illustration of the latched and unlatched states, showing how the latch mechanism controls energy storage and rapid release.

(C) Illustration of the latch-mediated energy release process divided into five distinct phases. The top row shows high-speed camera snapshots capturing the sequential motion, and the bottom rows illustrate the self-locking latch (i) and button latch (ii). Video S1 offers an overview of the complete process along with a slow-motion demonstration of MSEH operation.

(D) Velocity and displacement profiles of the magnet array throughout the entire process, highlighting the phase transition and high-speed acceleration.

(E and F) Zoomed-in displacement and velocity curves within phases I–III, demonstrating the dynamic details upon energy release.

Please cite this article in press as: Li et al., From nature's deadly strike to safety protection: Mantis shrimp-inspired ultrafast energy transformation for smart surveillance, Device (2025), https://doi.org/10.1016/j.device.2025.100903

images on the left in Figure 2B depict the latched and unlatched states of the mantis shrimp's appendage, offering a clear representation of how the latch system secures the appendage in preparation for the strike and how the energy is released when it transitions to an unlatched state. The simplified structures and schematics on the right provide a more detailed view of the mechanism, highlighting the function and operational states of the latch system during energy storage and release.

Inspired by the mantis shrimp's strike mechanism, we present a mechanically replicated design, referred to as an MSEH. As shown in Figure 2C, the MSEH can transform static loading into kinetic energy, manifested as ultrafast movement, and then convert it into electricity via electromagnetic induction. Similar to, yet distinct from, the biological latch system, our mechanical system features a two-part latch mechanism: a self-locking latch (Figure 2C-i) and a button latch (Figure 2C-ii). The self-locking latch works based on a mechanism that combines both spring tension and a button press to secure and release a system. When pressed, the button compresses the spring, moving a locking component into position to secure the latch in a locked state, preventing any unwanted movement or release. Pressing the button applies a force that compresses the spring and disengages the latch, allowing the locked parts to move freely. The button latch, as its name suggests, uses a button mechanism that, when pressed, compresses a spring. Once the force is removed, the button latch returns to and remains in the latched state. When a force is applied to the button—the silver part with an internal spring, as shown in the sequential images from 0 s to 0.2 s in Figure 2C-ii—a linkage mechanism will compress the wedge-shaped button in tandem, thereby releasing the component it previously blocked.

According to the biomechanical analysis of the mantis shrimp, its strike process can be divided into three phases. The working flow of our mechanism is more intricate and is divided into five phases. It is important to note that after the strike, the mantis shrimp's appendage cannot return to its initial latched state autonomously unless the extensor muscles contract again. Through a sophisticated design, our mechanical system not only mimics the energy storage and release mechanism observed in biological systems but also incorporates a self-reset feature (Figure S6), which is absent in nature. Unlike the mantis shrimp, which relies on active muscle contraction to relatch, our system autonomously resets via rebound and a dual-latch mechanism (Figure S1), representing a notable advancement over its biological counterpart. As shown in Figure 2C, the red and blue three-colored block furthest left, corresponding to the silver block in the subsequent images, consists of three magnet strips arranged in parallel. The magnet array is equivalent to the mantis shrimp's appendage, which is a movable structure that carries kinetic energy after the strike is conducted. Once the latch system is released, the stored energy is transferred to the magnet array, initiating ultrafast movement. This movement passes over the coils beneath, inducing electrical potentials in them.

At the beginning of phase I, the magnet array is firmly secured in its initial position by both the self-locking latch and the button latch, preventing any rightward motion and preparing it for elastic energy loading. Notably, the bottom housing, made of acrylic, features a two-part structure separated by reset springs, as shown in Figure 2C. During phase II, a horizontal force is applied to bring the two separate parts closer together, compressing both the buffer springs, which mimic the mantis shrimp's spring-loading behavior, and the reset springs separating the two parts of the bottom housing. During this phase, potential energy is gradually stored in the buffer springs. As depicted in Figures 2C-i and 2C-ii, the buttons of the two latch switches are being pressed. Once the relative horizontal distance between the two separate parts of the bottom housing decreases below a threshold, the system transitions into phase III, where the two latch switches are disengaged, allowing the magnet array to move freely to the right. The potential energy stored in the buffer springs is released and converted into the kinetic energy of the magnet array. Figure 2D presents the time-history responses of displacement and velocity for the magnet array throughout the entire cycle, highlighting the dynamic behavior during phases I–III and explicitly defining the rebound point, where the magnet array reaches its maximum displacement and the velocity momentarily drops to zero. Figures 2E and 2F offer close-up views of the displacement/velocity profiles across phases I–III. As demonstrated in Figure 2E, the velocity of the magnet array rapidly increases from the start of phase III. In the second half of phase III, after the magnet array reaches the rightmost boundary, it rebounds due to the impact with the rebound springs. Note that ball chutes are installed beneath the magnet array to minimize friction.

Phase IV begins with the re-engagement of the self-locking latch. As the magnet array rebounds and impacts the latch mechanism, it becomes securely hooked. Although the array is restrained, minor residual kinetic energy induces slight underdamped oscillations, as shown in Figure 2D. Phase V marks the final stage, initiated by the removal of the external force. The reset spring then actuates, returning the shell and button latch to their initial positions and preparing the system for the next cycle. Note S1 provides a detailed description of the five phases and the dual-latch mechanism, and a slow-motion video (Video S1) demonstrating the whole operation process is also available in the supplemental information. Throughout the whole process, it is clear that the magnet array carries substantial kinetic energy during phase III. Therefore, this phase is used for energy transformation. With three coils installed beneath the ball chutes, the passing magnet array induces electrical potentials via electromagnetic induction, which can then be collected by appropriate circuits. Figure S37 and Table S10 present the energy transformation within various components of the MSEH throughout its five operational phases.

Power capability characterization

Though not depicted in Figure 2, the bio-inspired energy harvester, MSEH, has a top cover integrating three additional coils to improve energy harvesting efficiency. This MSEH is further enclosed in specially designed structures (as shown in Figures S5–S8), which can convert the vertical force applied on the top of the structure into horizontal compression, thus triggering the bio-inspired kinetic amplification of the MSEH. The energy in the amplified kinetic motion is then converted

Please cite this article in press as: Li et al., From nature's deadly strike to safety protection: Mantis shrimp-inspired ultrafast energy transformation for smart surveillance, Device (2025), https://doi.org/10.1016/j.device.2025.100903

into electricity via electromagnetic induction. A finite element (FE) model was developed in ANSYS Maxwell, and Figure 3A shows the simulated magnetic field distribution, illustrating the magnet array's motion through alternating pole coils. Both the 3D and cross-sectional views highlight magnetic flux density, with stronger fields near the poles and coils. Figure 3B compares the simulated and experimentally measured voltage responses of six individual coils (coil #01 to coil #06) during a single impulse event.

Coils #01, #02, and #03 are embedded in the top cover, and coils #04, #05, and #06 are in the bottom housing. Due to symmetrical placement, voltage profiles are nearly identical across pairs, with variations mainly attributed to positional effects. For instance, coil #03, being near the right-hand-side boundary, exhibits clustered responses due to shorter induction intervals. Peak AC voltages exceed 60 V across coils. Figure 3C shows the peak power output of each coil under different load resistances. Maximum power (~7.74 W) occurs at ~610 Ω, matching the internal resistance of the coils for optimal energy transfer. Figure 3D depicts the force-displacement relationship before latch release. Applied force compresses buffer springs, storing energy until a critical displacement of ~9.14 mm and a force of ~296.9 N trigger the release. Figures 3E–3H show charging performance with different capacitors (47 μF–1 mF). Voltage profiles reveal slower charging for larger capacitors. The effective power decreases with increasing capacitance (Figure 3G). Fortunately, harvested energy (Figure 3F) is less sensitive. Maximum energy (~44.24 mJ) is achieved with a 100 μF capacitor. Figure 3H shows the corresponding charging times.

By replicating the bio-inspired latch-controlled mechanism, the MSEH ensures consistent output by storing a fixed amount of energy in buffer springs per trigger, regardless of excitation frequency or speed. This results in uniform kinetic energy release and thus consistent electrical output—even under slow, quasi-static excitations—enhancing robustness and efficiency. Two scenarios were designed to demonstrate consistency. In the first (Figure 3I), a single MSEH was integrated into a floor tile prototype (Figure S7) and tested with 10 volunteers (body weight: 59.4–100.5 kg). Despite varying body weights, voltage and energy outputs remained consistent, with maximum and minimum voltages of 27.25 and 25.74 V, corresponding to 37.68 and 33.14 mJ, respectively. Video S2 presents a demonstration of a single MSEH effectively powering real-world devices. In the second scenario (Figure 3J), four MSEHs were embedded in a larger floor tile (Figure S8) for vehicle testing. As a vehicle passed at various speeds, the MSEHs were reliably activated, converting mechanical input into electricity. Connected in parallel and paired with a 220 μF capacitor, the MSEHs produced voltage outputs ranging from 31.62 to 30.61 V and energy from 95.23 to 90.28 mJ. Although four units were used, the total energy harvested was less than four times that of a single unit due to circuit complexity, parasitic resistance, and asynchronous triggering. Notably, during each vehicle pass, the MSEHs were triggered twice—once by the front wheel and once by the rear. Taking both activations into account, the total energy harvested by the four MSEHs during a single pass was approximately 180 mJ. A demonstration of the system powering real-world loads is shown in Video S3.

Integration with an ultra-low-power radar system

Leveraging the mantis shrimp-inspired latch mechanism, the MSEH demonstrates high efficiency in converting ultra-slow motion into electricity, requiring only ~296.9 N of activation force—well below an average adult's body weight. This makes it suitable for event-triggered applications like intelligent transportation surveillance. In the first case study, MSEH units are utilized to power an ultra-low-power radar system for vehicle detection. Figure 4A demonstrates the radar sensor's directional performance under two placements: horizontal and elevated (3 m). The elevated setup provides significantly better coverage and thus was adopted for field deployment.

Figure 4B outlines the radar system's working principle. When no vehicle is within 7 m (scenario i), the radar remains on standby. If a vehicle enters within 7 m (scenario ii), the radar activates and triggers a Bluetooth alert to nearby pedestrians, enhancing safety in areas with visual obstructions. Figure 4C illustrates the operating sequence: once activated by harvested energy, the radar system powers on, completes a 3-s self-test, and enters detection mode. If a target is detected, Bluetooth communication is triggered to transmit warning signals, which are displayed on users' mobile devices. After the vehicle exits the sensing range, the radar enters a short lockout period before resetting.

Figure 4D and Video S4 demonstrate a real-world implementation, where eight MSEH units are integrated into a power-generating floor installed beneath a speed bump. The MSEHs are divided into two groups positioned on either side of the bump, ensuring that each wheel (left or right) activates one group as it passes. Since the energy from four MSEH units is sufficient for the power supply, only one group was connected to the circuit during testing, while the other served as a backup. The harvested energy powers a radar sensor that detects vehicles and communicates warnings. Figure 4D-iv illustrates the specific application scenario, where a narrow pedestrian pathway, as indicated by the yellow arrow, intersects with a roadway, as indicated by the white arrow. As highlighted, a visual blind spot obstructs the line of sight between pedestrians and approaching vehicles, posing a potential safety risk.

Although MSEHs are efficient, the energy harvested from a passing vehicle is still limited. Therefore, the radar system must be engineered for ultra-low-power operation. Figure 4E presents the circuit architecture, including the energy management unit (EMU), microwave radar sensor, microcontroller unit (MCU), and Bluetooth module. The AC output from the MSEH units is rectified to DC and then managed by the EMU (based on LTC3588-1), which stabilizes the voltage and prevents premature power delivery by an under-voltage lockout (UVLO) feature. The EMU is essential for ensuring the efficient and safe utilization of the harvested energy. Without it, the rapid charging of the storage capacitor could result in voltage surges that may irreversibly damage downstream electronics. In this work, the LTC3588-1 module was configured with UVLO settings, including a turn-on threshold voltage of 4.73 V, a turn-off threshold voltage of 3.67 V, and a regulated output voltage of 3.3 V. After the MSEH is triggered, the storage voltage rises rapidly. Once it exceeds the turn-on threshold, the UVLO function activates and supplies a stable 3.3 V to a 5.8 GHz radar

Please cite this article in press as: Li et al., From nature's deadly strike to safety protection: Mantis shrimp-inspired ultrafast energy transformation for smart surveillance, Device (2025), https://doi.org/10.1016/j.device.2025.100903

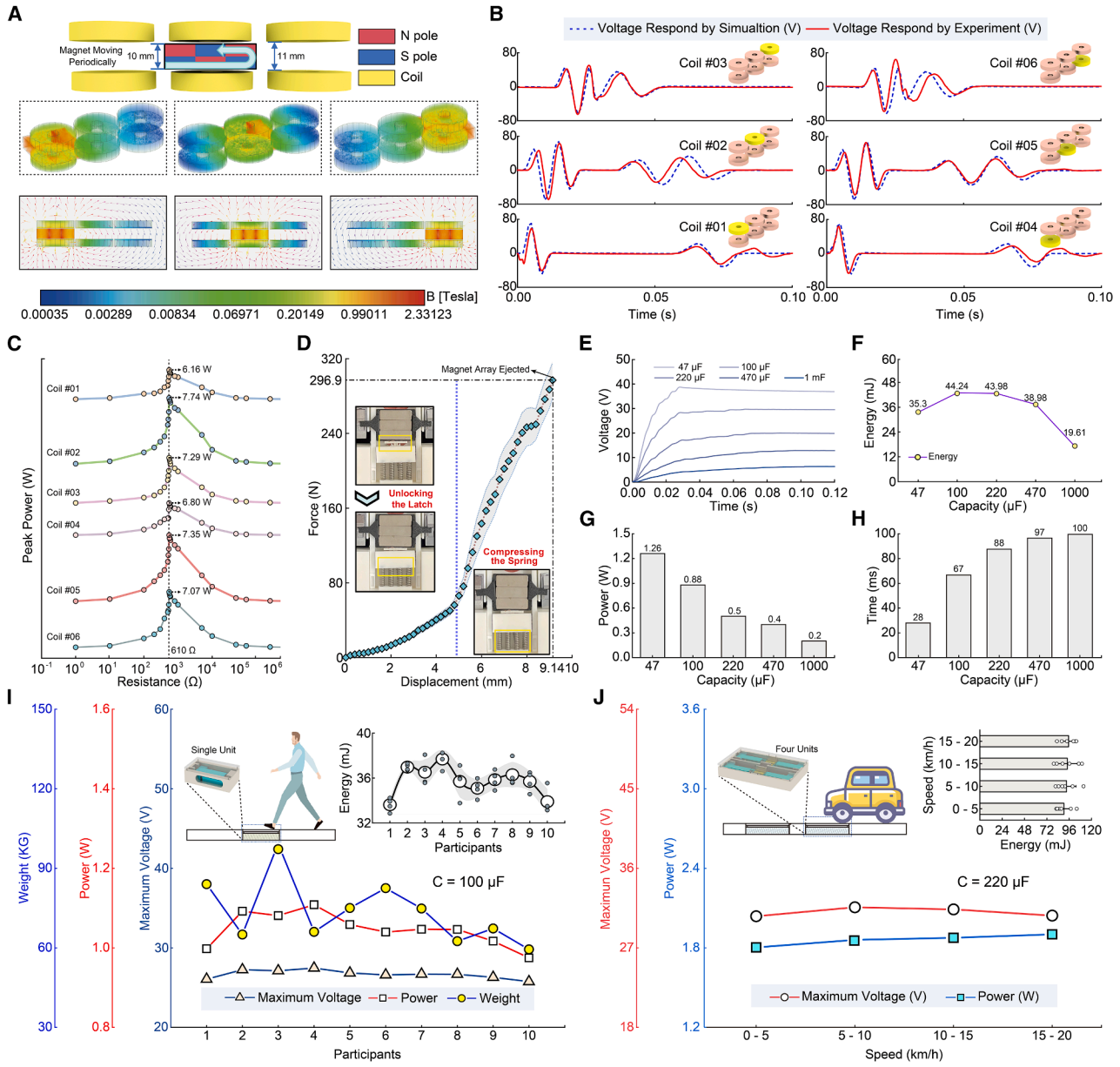

Figure 3. Performance evaluation of the mantis shrimp-inspired energy harvester

(A) Schematic illustration and magnetic field simulation of the mantis shrimp-inspired energy harvester (MSEH), showing the motion of the magnet array passing through coils and the corresponding magnetic flux distribution.

(B) Measured and simulated voltage responses from six coils, confirming good agreement and illustrating the oscillatory nature of the output.

(C) Peak power output across a range of load resistances for each coil, revealing optimal load conditions.

(D) Force-displacement relationship (presented as mean ± standard deviation) of the magnet array before energy release, depicting the potential energy loading process and the critical displacement and force required to trigger latch off.

(E) Voltage charging profiles under different capacitor values (47 μF–1 mF), showing the energy storage dynamics of the system.

(F and G) Harvested energy and effective power across different capacitors.

(H) Charging time required to reach voltage saturation for different capacitors.

(I) Power generation performance of a single MSEH unit under human walking conditions with varying body weights, demonstrating slight variations in voltage, power, and energy output (presented as ± standard deviation) among participants. Video S2 demonstrates the capability of a single MSEH to power real-world loads.

(J) Power generation performance of a four-unit MSEH system under vehicle loads at different speeds, showing slight fluctuations in voltage, power, and energy output (presented as ± standard deviation) across different vehicle speeds. Video S3 presents a real-world demonstration of using a four-unit MSEH system to power external loads.

Please cite this article in press as: Li et al., From nature's deadly strike to safety protection: Mantis shrimp-inspired ultrafast energy transformation for smart surveillance, Device (2025), https://doi.org/10.1016/j.device.2025.100903

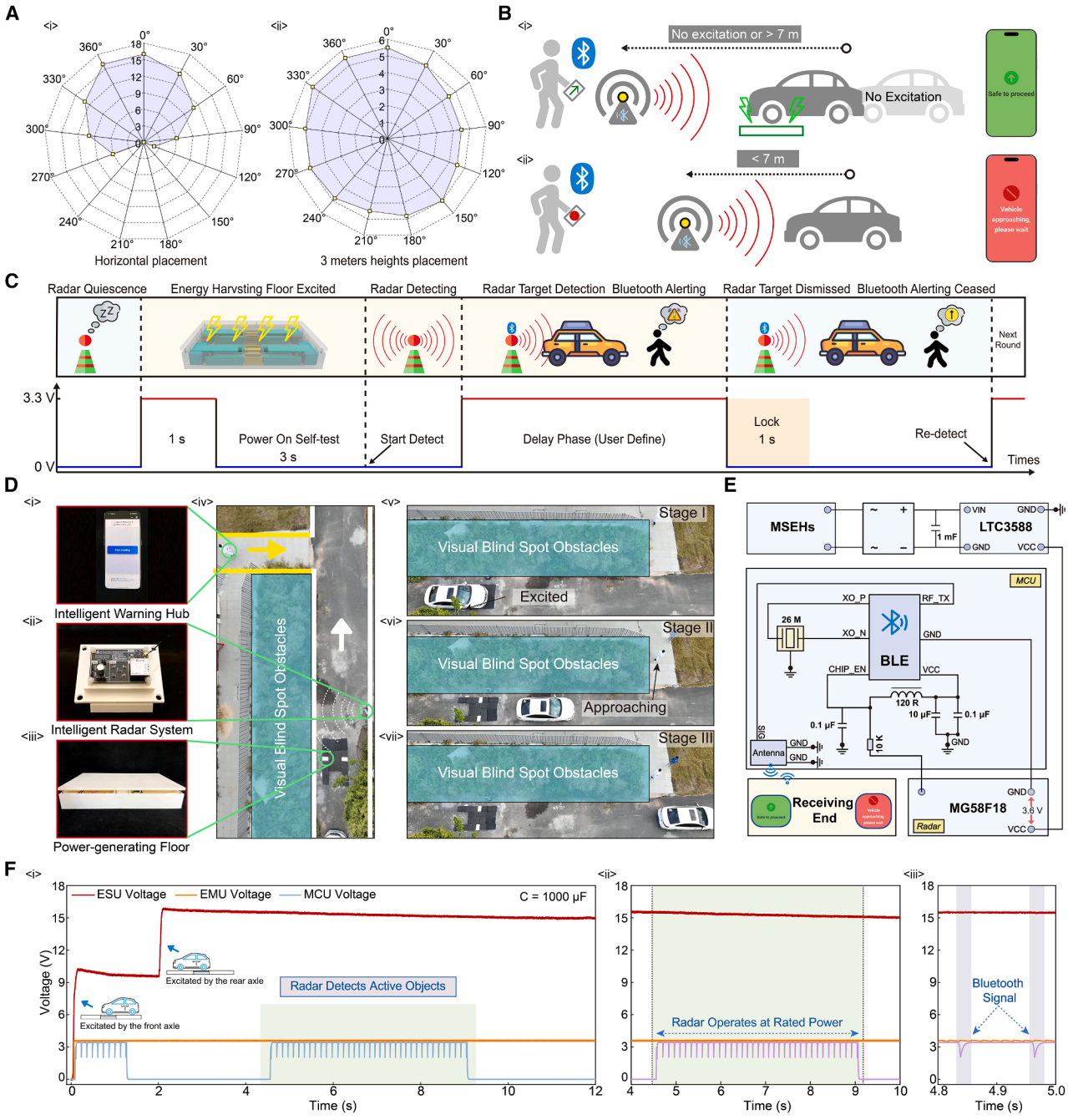

Figure 4. Integration of the mantis shrimp-inspired energy harvester with an ultra-low power radar

(A) Radar characterization under two placement conditions. (i) Horizontal placement. (ii) Elevated placement at 3 m, showing improved angular coverage.

(B) Working principle of the radar system. (i) No excitation or vehicle detected beyond 7 m—safe to proceed. (ii) A vehicle is detected within 7 m, triggering radar and Bluetooth alerting.

(C) Timing diagram illustrating the system's workflow: energy harvesting triggers radar activation, followed by object detection, Bluetooth alerting, a lock period, and system reset for the next cycle.

(D) System components and real-world deployment. (i) Intelligent warning hub for user notifications. (ii) Intelligent radar system. (iii) Power-generating floor embedded with mantis shrimp-inspired energy harvester (MSEH) units. (iv–vi) Aerial photographs showing the system in action: stage I (excited), stage II (approaching), and stage III (safe to proceed). Video S4 shows the field test of the intelligent radar system.

(E) Circuit architecture of the integrated system, including the energy management unit (EMU), microcontroller unit (MCU), Bluetooth module, and radar sensor.

(F) Experimental results. (i) Voltage profiles of the energy storage unit (ESU), EMU, and MCU during vehicle passage, with dual excitations from the front and rear axles. (ii) Radar operating at rated voltage. (iii) Bluetooth transmission initiated after vehicle detection.

Please cite this article in press as: Li et al., From nature's deadly strike to safety protection: Mantis shrimp-inspired ultrafast energy transformation for smart surveillance, Device (2025), https://doi.org/10.1016/j.device.2025.100903

CellPress
OPEN ACCESS

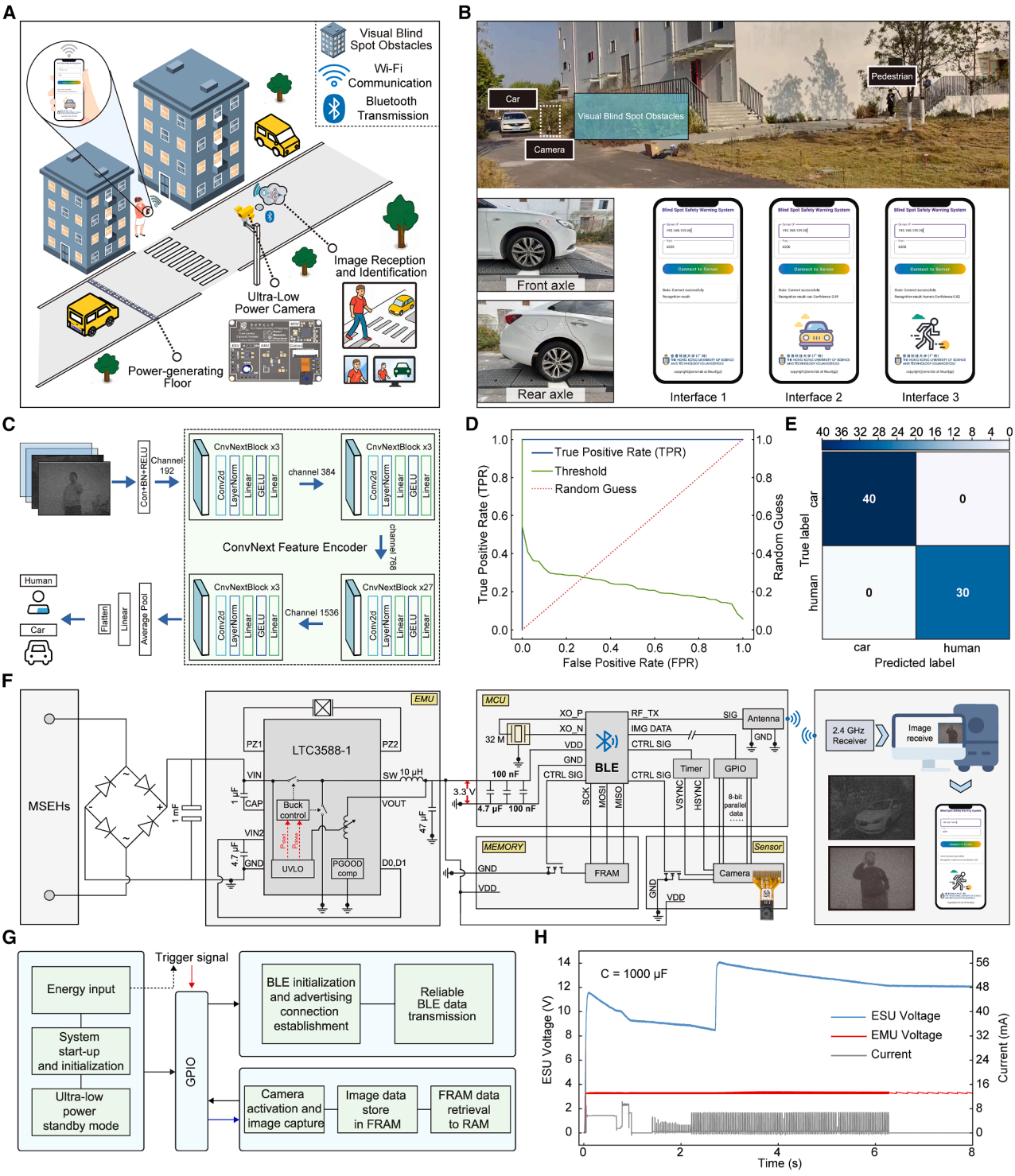

Figure 5. Integration of the mantis shrimp-inspired energy harvester with an intelligent camera system

(A) Conceptual illustration of the upgraded intelligent camera system, which includes mantis shrimp-inspired energy harvester (MSEH) units, an image sensor, a wireless transmission module, and a deep-learning-based recognition system.

(B) Real-world deployment, showing the installation of the camera module near visual blind spot obstacles and three different user interfaces: interface 1 (standby), interface 2 (vehicle detected), and interface 3 (pedestrian detected). Video S5 provides a demonstration of the intelligent camera system under field test conditions.

(legend continued on next page)

Please cite this article in press as: Li et al., From nature's deadly strike to safety protection: Mantis shrimp-inspired ultrafast energy transformation for smart surveillance, Device (2025), https://doi.org/10.1016/j.device.2025.100903

sensor (Magortek MG58F18), which remains idle until a target is detected. Upon detection, the EMU outputs a PGOOD signal to wake up the MCU (Nordic NRF52832) with integrated Bluetooth Low Energy (BLE), which then broadcasts a warning message to nearby devices via a mobile app. During the broadcasting process, the electronic components consume relatively high power. Once the stored energy is depleted and the capacitor voltage drops below the defined UVLO threshold, the EMU cuts the regulated output, thereby interrupting the power supply to prevent unstable operation and protect the system. Nearby receivers, such as a mobile phone running a customized application, receive the message and display the detection result and alerts (e.g., green for "no detection" and red for "vehicle detected"). The graphical user interface (GUI) of the mobile application is shown on the right in Figure 4B, with zoomed-in views provided in Figure S26.

Figure 4F presents the voltage and current characteristics of the system over time, illustrating the energy storage, output stabilization, and system activation process. The red curve represents the voltage across the energy storage unit (ESU), which exhibits two distinct surges in response to excitations from the vehicle's front and rear axles. The orange curve represents the stabilized output voltage from the EMU. The EMU voltage remains at zero and rises to, then stabilizes at, 3.6 V once the ESU voltage exceeds a critical threshold of 5.05 V. The light blue curve indicates the output voltage of the radar sensor (rated at 3.6 V), which is used as the MCU's input voltage. For most of the time, the MCU voltage remains at zero, indicating no target detection and, thus, no power consumption. Once a vehicle is detected, the MCU is powered on and drives the BLE module to broadcast warning messages with a time interval of 100 ms. In Figure 4F-ii, the radar operates at its rated voltage, as indicated by the orange curve, representing the stable supply voltage from the EMU. Figure 4F-iii presents a detailed view of the voltage dynamics during BLE transmission, showing periodic drops due to the power consumption of the MCU. When the MCU is activated, it draws power from this voltage source, resulting in a noticeable voltage decline due to the lack of a stabilization mechanism at the output pins of the radar sensor. Overall, Figure 4F illustrates the system's dynamic power utilization. Video S4 showcases the field test of this intelligent radar system.

Integration with an intelligent camera system

While the radar-based system performed well, it cannot distinguish between vehicles and pedestrians. To address this limitation, an ultra-low-power camera system powered by MSEH units is developed to enable intelligent object recognition and enhance situational awareness in low-visibility areas. As shown in Figure 5A, the system integrates eight MSEH units embedded in a speed bump, with four connected to the harvesting circuit and the remaining reserved as backups. Upon activation by passing vehicles, the connected MSEH units generate electricity to power a roadside ultra-low-power camera. The camera captures an image of the approaching object and transmits it via BLE to an edge-processing terminal. A deep learning model implemented on the terminal processor classifies the object as either a vehicle or a pedestrian. If a vehicle is detected, a warning alert is broadcast to nearby mobile devices via Wi-Fi or 5G, enabling real-time hazard alerts.

Figure 5B and Video S5 show the real-world deployment of the system, including camera installation near visual blind spots and the three user interface states: standby, vehicle detected, and pedestrian detected. The system utilizes a pre-trained ConvNeXt deep learning model (Figure 5C) for object recognition. Figure 5D presents the deep learning model's receiver operating characteristic (ROC) curve, indicating high accuracy with a true positive rate significantly above a random classification. As shown in the confusion matrix (Figure 5E), the model achieved 100% accuracy, correctly classifying all 40 vehicle and 30 pedestrian images. Video S6 further demonstrates the correct identification of vehicles and pedestrians in real-world scenarios.

The camera system is designed for ultra-low-power operation (Figure 5F), using the same EMU and MCU as for the radar system. A CMOS image sensor connects to the MCU via an 8-bit parallel data bus. The MCU operates at a 32 kHz clock rate to minimize power consumption, and the camera captures images at a lower 162 $\times$ 121 resolution, which reduces both processing load and energy usage. Preliminary analysis shows that under a steady 3.3 V power supply, the camera system consumes about 38.41 mJ per image capture and transmission cycle, as shown in Figure S31. However, when powered by MSEHs, the energy requirement increases to $\sim$60 mJ per cycle due to power conversion losses, voltage fluctuations, and repeated initialization. Still, given that four MSEH units generate over 90 mJ, the energy supply is more than sufficient.

Figure 5G illustrates the embedded system architecture and workflow designed to achieve ultra-low-power operation. The system is awakened by an energy input from the MSEH units, followed by startup and initialization. Then, the MCU enters an ultra-low-power standby mode. GPIO ports are configured to activate system functions. The system then follows two primary operational paths: one dedicated to BLE communication and the other to image capture. The upper path manages BLE initialization, advertising, and reliable data transmission. The lower path oversees image acquisition, where the camera is activated to capture images, which are first stored in ferroelectric RAM (FRAM) to conserve energy and preserve data integrity. Once completed, the image data are

(C) Image recognition pipeline employing a ConvNeXt feature encoder for classifying captured scenes as either vehicles or pedestrians. Video S6 shows the image content recognition process on the receiving terminal.
(D) Receiver operating characteristic (ROC) curve showing the classification performance of the model.
(E) Confusion matrix demonstrating high classification accuracy, with all 40 car images and all 30 human images correctly identified.
(F) Circuit architecture of the entire system, incorporating an energy management unit (EMU), a microcontroller unit (MCU), a camera module, and a wireless communication module.
(G) Embedded system programming workflow demonstrating how ultra-low-power operation is achieved, including event-triggered image capture, memory handling, and BLE communication.
(H) Experimental results from the field test, showing ESU voltage, EMU output voltage, and current consumption over time during a complete operating cycle.

Please cite this article in press as: Li et al., From nature's deadly strike to safety protection: Mantis shrimp-inspired ultrafast energy transformation for smart surveillance, Device (2025), https://doi.org/10.1016/j.device.2025.100903

retrieved from FRAM and transferred to the RAM of the MCU, which is prepared for transmission. This energy-efficient architecture allows power-intensive tasks—such as image capture and wireless transmission—to be executed only when necessary, thereby minimizing overall energy consumption.

Figure 5H presents the results of a field test, revealing the voltage and current dynamics of the system during operation upon being triggered. The energy collection process, characterized by the two-stage increase in the ESU voltage curve, is similar to that in Figure 4F. The ESU voltage first increases, followed by a gradual decline, indicating continuous power consumption. Once the ESU voltage rises above a predefined threshold, the EMU begins supplying a stable output voltage. Some initial current spikes—attributed to the MCU's startup behavior—are followed by pulsed activity between 2 and 6 s, corresponding to the operation of the MCU, camera, and BLE module. These field test results prove the feasibility and effectiveness of integrating MSEH-powered intelligent camera systems for real-time, self-powered object recognition and hazard alerting in transportation environments. Video S5 showcases the field test of this intelligent camera system.

Conclusion

In this work, we presented the design of an MSEH that replicates and enhances the biomechanics of the mantis shrimp's strike for high-efficiency energy conversion. By employing a latch-mediated energy storage and release mechanism, the MSEH transforms slow external forces into ultrafast motion and then into electricity, exhibiting remarkably higher power density than existing designs. Performance characterization showed that the MSEH generates a peak voltage of 60 V, with a maximum instantaneous power output of 7.74 W. Under a single impulse excitation, a single MSEH unit can generate up to 44.24 mJ energy when charging a 100 μF capacitor. To validate and showcase its practicality, we utilized multiple MSEH units to develop a battery-free intelligent surveillance system for enhancing safety in transportation, where they successfully powered an ultra-low-power radar sensor and a camera-based object recognition system. Our field tests demonstrated that four MSEH units embedded in a speed bump could provide sufficient energy (~180 mJ) to sustain the operation of both the radar and the camera monitoring system (~60 mJ). A smart terminal deployed with a pre-trained deep learning model received the image from the camera system and analyzed the content. The deep-learning-based image recognition model demonstrated a high classification accuracy, accurately distinguishing 40 vehicles and 30 pedestrians. The intelligent terminal then relayed real-time alerts to nearby users and displayed them on mobile devices, enhancing safety in visually obstructed scenarios. The findings in this work highlight the promising potential of bio-inspired kinetic energy harvesting as a scalable solution for energy-autonomous sensing and monitoring in intelligent transportation contexts.

METHODS

FE simulation model

An FE model was developed for simulating the magnet array motion and the induced electrical potential in the coils. In ANSYS Maxwell, the "zero tangential H field" boundary condition was adopted to control the magnetic field behavior. This condition forces the magnetic field lines to remain perpendicular to the boundary, effectively confining the field within specified domains and simplifying computation by preventing field extension beyond the boundary. It was applied to the outer boundaries of the FE model to simulate a non-magnetic surrounding environment (e.g., air or vacuum), where no tangential magnetic field is expected.

After comparison with the properties from suppliers, suitable material models were chosen from the material library provided in ANSYS Maxwell for simulation. The properties of copper (the material of coils), including its relative permeability (0.99991) and bulk conductivity (5.8×10^7 S/m), are standard values commonly used for electromagnetic simulations. Neodymium iron boron magnets were assigned typical properties, with a relative permeability of 1.47 and a magnetic coercivity of −730,000 A/m. The vacuum properties, featuring a relative permeability of 1.0000004 and zero bulk conductivity, conform to standard parameters for non-conductive electromagnetic simulations. The software intelligently selects the appropriate element types based on the simulation setup and the specific analysis.

Prototyping and assembly

To fabricate the MSEH units, we employed 3D printing technology for rapid prototyping. Using a Bambu Lab X1E 3D printer, we printed the structural components with high-strength polymer materials (PAHT-CF), ensuring precise replication of the designed latch-mediated energy storage and release mechanism. The printed components were post-processed and assembled with other mechanical and electromagnetic elements, including the buffer springs, permanent magnets (neodymium iron boron), and copper coils for energy conversion. The self-locking and button latch mechanisms were carefully integrated to mimic the biomechanical strike mechanism of the mantis shrimp. Once assembled, the MSEH units were tested for mechanical integrity and alignment to ensure their proper functionalities before experimental evaluation.

Measurement and testing procedures

A series of tests was conducted under controlled conditions to comprehensively evaluate the performance of the prototyped MSEH. The mechanical response of the MSEH was characterized by applying single impulse excitations to activate the latch-mediated release mechanism, during which the velocity and displacement of the magnet array were measured using a high-speed camera (Photron Nova S16) and a laser Doppler sensor (SOPTOP LV-S01). The electrical performance was assessed by measuring the induced voltage across the coils with a multi-channel oscilloscope (RIGOL DHO 1104), a data acquisition system (NI DAQ card), and an electrometer (Keithley 6517B) to ensure high accuracy. Additionally, the energy storage capability and conversion efficiency of the system were evaluated by testing the charging behavior of capacitors with different values (47 μF, 100 μF, 220 μF, 470 μF, and 1 mF).

RESOURCE AVAILABILITY

Lead contact

Requests for further information and resources should be directed to and will be fulfilled by the lead contact, Guobiao Hu (guobiaohu@hkust-gz.edu.cn).

Materials availability

This study did not generate new, unique reagents.

Data and code availability

The data and code that support the conclusions of this study are also available from the lead contact upon reasonable request.

ACKNOWLEDGMENTS

This study was financially supported in part by the National Natural Science Foundation of China (grant no. 52305135); the Guangzhou Municipal Science and Technology Bureau (grant nos. SL2023A03J00869 and SL2023A04 J01741); the Guangdong Provincial Key Lab of Integrated Communication, Sensing and Computation for Ubiquitous Internet of Things (grant no. 2023B1212010007); and the Guangzhou Municipal Key Laboratory on Future Networked Systems (grant no. 024A03J0623). Acknowledgment is also given to Freepik (www.freepik.com) for providing open-source graphic resources.

AUTHOR CONTRIBUTIONS

G.H. conceived the idea, drafted the manuscript, and secured the funding. Yihao Li, Yizhou Li, and Y.W. designed the experiment and prepared the figures. Yihao Li and Yizhou Li conducted the test and measurements and collected the data. M.X. and H.T. designed and developed the circuit boards. Y.Z., J. W., X.L., W.-H.L., and G.H. polished the manuscript. G.H. supervised and guided the project.

DECLARATION OF INTERESTS

The authors declare no conflicts of interest.

SUPPLEMENTAL INFORMATION

Supplemental information can be found online at https://doi.org/10.1016/j.device.2025.100903.

Received: May 8, 2025
Revised: July 21, 2025
Accepted: July 29, 2025

REFERENCES

1. Patek, S.N., Korff, W.L., and Caldwell, R.L. (2004). Biomechanics: deadly strike mechanism of a mantis shrimp. Nature *428*, 819–820. https://doi.org/10.1038/428819a.
2. Crane, R.L., Cox, S.M., Kisare, S.A., and Patek, S.N. (2018). Smashing mantis shrimp strategically impact shells. J. Exp. Biol. *221*, jeb176099. https://doi.org/10.1242/jeb.176099.
3. Tang, X., and Staack, D. (2019). Bioinspired mechanical device generates plasma in water via cavitation. Sci. Adv. *5*, eaau7765. https://doi.org/10.1126/sciadv.aau7765.
4. Patek, S. (2015). The most powerful movements in biology: from jellyfish stingers to mantis shrimp appendages, it takes more than muscle to move extremely fast. Am. Sci. *103*, 330–338. https://doi.org/10.1511/2015.116.330.
5. Steinhardt, E., Hyun, N.-s.P., Koh, J.-s., Freeburn, G., Rosen, M.H., Temel, F.Z., Patek, S.N., and Wood, R.J. (2021). A physical model of mantis shrimp for exploring the dynamics of ultrafast systems. Proc. Natl. Acad. Sci. USA *118*, e2026833118. https://doi.org/10.1073/pnas.2026833118.
6. Patek, S.N., and Caldwell, R.L. (2005). Extreme impact and cavitation forces of a biological hammer: strike forces of the peacock mantis shrimp Odontodactylus scyllarus. J. Exp. Biol. *208*, 3655–3664. https://doi.org/10.1242/jeb.01831.
7. Alderete, N.A., Sandeep, S., Raetz, S., Asgari, M., Abi Ghanem, M., and Espinosa, H.D. (2025). Does the mantis shrimp pack a phononic shield? Science *387*, 659–666. https://doi.org/10.1126/science.adq7100.
8. deVries, M.S., Murphy, E.A.K., and Patek, S.N. (2012). Strike mechanics of an ambush predator: the spearing mantis shrimp. J. Exp. Biol. *215*, 4374–4384. https://doi.org/10.1242/jeb.075317.
9. Tadayon, M., Amini, S., Wang, Z., and Miserez, A. (2018). Biomechanical Design of the Mantis Shrimp Saddle: A Biomineralized Spring Used for Rapid Raptorial Strikes. iScience *8*, 271–282. https://doi.org/10.1016/j.isci.2018.08.022.
10. Harrison, J.S., Porter, M.L., McHenry, M.J., Robinson, H.E., and Patek, S. N. (2021). Scaling and development of elastic mechanisms: the tiny strikes of larval mantis shrimp. J. Exp. Biol. *224*, jeb235465. https://doi.org/10.1242/jeb.235465.
11. Patek, S.N., Nowroozi, B.N., Baio, J.E., Caldwell, R.L., and Summers, A.P. (2007). Linkage mechanics and power amplification of the mantis shrimp's strike. J. Exp. Biol. *210*, 3677–3688. https://doi.org/10.1242/jeb.006486.
12. Zack, T.I., Claverie, T., and Patek, S.N. (2009). Elastic energy storage in the mantis shrimp's fast predatory strike. J. Exp. Biol. *212*, 4002–4009. https://doi.org/10.1242/jeb.034801.
13. Ilton, M., Bhamla, M.S., Ma, X., Cox, S.M., Fitchett, L.L., Kim, Y., Koh, J.-s., Krishnamurthy, D., Kuo, C.-Y., Temel, F.Z., et al. (2018). The principles of cascading power limits in small, fast biological and engineered systems. Science *360*, eaao1082. https://doi.org/10.1126/science.aao1082.
14. Ito, F., Ishii, Y., Kurumaya, S., Kagaya, K., and Nakamura, T. (2022). Instantaneous Force Generation Mechanism Based on the Striking Motion of Mantis Shrimp-Design and Control Method of Cavitation by Simulation and Experiment. IEEE Robot. Autom. Lett. *7*, 9342–9349. https://doi.org/10.1109/Lra.2022.3190614.
15. Li, X., Li, X., Hou, X., Li, Y., Meng, Y., Ma, L., and Tian, Y. (2022). Mantis Shrimp-Inspired Underwater Striking Device Generates Cavitation. J. Bionic Eng. *19*, 1758–1770. https://doi.org/10.1007/s42235-022-00227-8.
16. Burgess, S. (2021). A review of linkage mechanisms in animal joints and related bioinspired designs. Bioinspir. Biomim. *16*, 041001. https://doi.org/10.1088/1748-3190/abf744.
17. Zhang, B., Xu, W., Peng, L., Li, Y., Zhang, W., and Wang, Z. (2024). Nature-inspired interfacial engineering for energy harvesting. Nat. Rev. Electr. Eng. *1*, 218–233.
18. Chen, W., Lu, Y., Li, S., and Gao, F. (2023). A bio-inspired foldable-wing wave energy converter for ocean robots. Appl. Energy *334*, 120696. https://doi.org/10.1016/j.apenergy.2023.120696.
19. Maiti, S., Karan, S.K., Kim, J.K., and Khatua, B.B. (2019). Nature Driven Bio-Piezoelectric/Triboelectric Nanogenerator as Next-Generation Green Energy Harvester for Smart and Pollution Free Society. Adv. Energy Mater. *9*, 1803027. https://doi.org/10.1002/aenm.201803027.
20. Jin, C., Zhang, C., Yan, P., Jiang, M., Yin, R., Li, K., Zhao, W., and Bai, Z. (2024). A Superhuman Sensing Triboelectric Nanogenerator with Boosted Power Density and Durability via a Bio-Inspired Janus Structure. Adv. Funct. Mater. *34*, 2402233. https://doi.org/10.1002/adfm.202402233.
21. Zhou, H., Li, D., He, X., Hui, X., Guo, H., Hu, C., Mu, X., and Wang, Z.L. (2021). Bionic Ultra-Sensitive Self-Powered Electromechanical Sensor for Muscle-Triggered Communication Application. Adv. Sci. *8*, 2101020. https://doi.org/10.1002/advs.202101020.
22. Patek, S.N. (2023). Latch-mediated spring actuation (LaMSA): the power of integrated biomechanical systems. J. Exp. Biol. *226*, jeb245262. https://doi.org/10.1242/jeb.245262.

23. Rosario, M.V., Sutton, G.P., Patek, S.N., and Sawicki, G.S. (2016). Muscle–spring dynamics in time-limited, elastic movements. Proc. Biol. Sci. *283*, 20161561. https://doi.org/10.1098/rspb.2016.1561.

24. Ribak, G. (2020). Insect-inspired jumping robots: challenges and solutions to jump stability. Curr. Opin. Insect Sci. *42*, 32–38. https://doi.org/10.1016/j.cois.2020.09.001.

25. Aubin, C.A., Gorissen, B., Milana, E., Buskohl, P.R., Lazarus, N., Slipher, G.A., Keplinger, C., Bongard, J., Iida, F., Lewis, J.A., and Shepherd, R.F. (2022). Towards enduring autonomous robots via embodied energy. Nature *602*, 393–402. https://doi.org/10.1038/s41586-021-04138-2.

26. Gao, Q., Jing, Z., Sun, Y., Zhang, S., Gu, C., Ma, L., Li, H., Wen, J., Cheng, X., and Cheng, T. (2024). Bionic Fish-Shaped Triboelectric-Electromagnetic Hybrid Generator via a Two-Stage Swing Mechanism for Water Flow Energy Harvesting and Condition Monitoring. ACS Appl. Mater. Interfaces *16*, 569–575. https://doi.org/10.1021/acsami.3c13690.

27. Zhang, S., Jing, Z., Wang, X., Fan, K., Zhao, H., Wang, Z.L., and Cheng, T. (2022). Enhancing Low-Velocity Water Flow Energy Harvesting of Triboelectric-Electromagnetic Generator via Biomimetic-Fin Strategy and Swing-Rotation Mechanism. ACS Energy Lett. *7*, 4282–4289. https://doi.org/10.1021/acsenergylett.2c01908.

28. Tao, K., Yi, H., Yang, Y., Chang, H., Wu, J., Tang, L., Yang, Z., Wang, N., Hu, L., Fu, Y., et al. (2020). Origami-inspired electret-based triboelectric generator for biomechanical and ocean wave energy harvesting. Nano Energy *67*, 104197. https://doi.org/10.1016/j.nanoen.2019.104197.

29. Xiao, X., Mei, Y., Deng, W., Zou, G., Hou, H., and Ji, X. (2024). Electric Eel Biomimetics for Energy Storage and Conversion. Small Methods *8*, e2201435. https://doi.org/10.1002/smtd.202201435.

30. Li, J., Du, L., Kong, X., Wu, J., Lu, D., Jiang, L., and Guo, W. (2023). Designing artificial ion channels with strict K(+)/Na(+) selectivity toward next-generation electric-eel-mimetic ionic power generation. Natl. Sci. Rev. *10*, nwad260. https://doi.org/10.1093/nsr/nwad260.

31. Wang, C., Choi, E., and Park, J. (2018). High-voltage nanofluidic energy generator based on ion-concentration-gradients mimicking electric eels. Nano Energy *43*, 291–299. https://doi.org/10.1016/j.nanoen.2017.11.054.

32. Patek, S.N., Baio, J.E., Fisher, B.L., and Suarez, A.V. (2006). Multifunctionality and mechanical origins: ballistic jaw propulsion in trap-jaw ants. Proc. Natl. Acad. Sci. USA *103*, 12787–12792. https://doi.org/10.1073/pnas.0604290103.

33. Burrows, M. (2003). Biomechanics: froghopper insects leap to new heights. Nature *424*, 509. https://doi.org/10.1038/424509a.

34. Bennet-Clark, H.C. (1975). The energetics of the jump of the locust Schistocerca gregaria. J. Exp. Biol. *63*, 53–83. https://doi.org/10.1242/jeb.63.1.53.

35. Sharp, N.C.C. (1997). Timed running speed of a cheetah (Acinonyx jubatus). J. Zool. *241*, 493–494. https://doi.org/10.1111/j.1469-7998.1997.tb04840.x.

36. Weyand, P.G., Lin, J.E., and Bundle, M.W. (2006). Sprint performance-duration relationships are set by the fractional duration of external force application. Am. J. Physiol. Regul. Integr. Comp. Physiol. *290*, R758–R765. https://doi.org/10.1152/ajpregu.00562.2005.

37. Koh, J.S., Yang, E., Jung, G.P., Jung, S.P., Son, J.H., Lee, S.I., Jablonski, P.G., Wood, R.J., Kim, H.Y., and Cho, K.J. (2015). BIOMECHANICS. Jumping on water: Surface tension-dominated jumping of water striders and robotic insects. Science *349*, 517–521. https://doi.org/10.1126/science.aab1637.

38. Burrows, M. (2012). Jumping mechanisms in jumping plant lice (Hemiptera, Sternorrhyncha, Psyllidae). J. Exp. Biol. *215*, 3612–3621. https://doi.org/10.1242/jeb.074682.

39. Nuchter, T., Benoit, M., Engel, U., Ozbek, S., and Holstein, T.W. (2006). Nanosecond-scale kinetics of nematocyst discharge. Curr. Biol. *16*, R316–R318. https://doi.org/10.1016/j.cub.2006.03.089.

40. Edwards, J., Whitaker, D., Klionsky, S., and Laskowski, M.J. (2005). Botany: a record-breaking pollen catapult. Nature *435*, 164. https://doi.org/10.1038/435164a.

41. Vincent, O., Weisskopf, C., Poppinga, S., Masselter, T., Speck, T., Joyeux, M., Quilliet, C., and Marmottant, P. (2011). Ultra-fast underwater suction traps. Proc. Biol. Sci. *278*, 2909–2914. https://doi.org/10.1098/rspb.2010.2292.

42. Yin, P., Tang, L., Li, Z., Xia, C., Li, Z., and Aw, K.C. (2025). Harnessing ultra-low-frequency vibration energy by a rolling-swing electromagnetic energy harvester with counter-rotations. Appl. Energy *377*, 124507. https://doi.org/10.1016/j.apenergy.2024.124507.

43. Zou, H.-X., Zhu, Q.-W., He, J.-Y., Zhao, L.-C., Wei, K.-X., Zhang, W.-M., Du, R.-H., and Liu, S. (2024). Energy harvesting floor using sustained-release regulation mechanism for self-powered traffic management. Appl. Energy *353*, 122082. https://doi.org/10.1016/j.apenergy.2023.122082.

44. Cai, M., and Liao, W.H. (2021). Enhanced electromagnetic wrist-worn energy harvester using repulsive magnetic spring. Mech. Syst. Signal Process. *150*, 107251. https://doi.org/10.1016/j.ymssp.2020.107251.

45. Liu, S., Liao, S., Liu, D., Qing, W., Wei, K., Zhao, L., and Zou, H. (2024). A compact hybridized triboelectric-electromagnetic road energy harvester for vehicle speed measurement. DeCarbon *3*, 100036. https://doi.org/10.1016/j.decarb.2024.100036.

46. Li, Y., Peng, X., Li, Y., Li, D., and Hu, G. (2025). Catapult mechanism-enabled push-button energy harvester designed for capturing ultra-low frequency motion. Mech. Syst. Signal Process. *225*, 112268. https://doi.org/10.1016/j.ymssp.2024.112268.

47. Zhang, K., Wang, X., Yang, Y., and Wang, Z.L. (2015). Hybridized electromagnetic-triboelectric nanogenerator for scavenging biomechanical energy for sustainably powering wearable electronics. ACS Nano *9*, 3521–3529. https://doi.org/10.1021/nn507455f.

48. Smilek, J., Hadas, Z., Vetiska, J., and Beeby, S. (2019). Rolling mass energy harvester for very low frequency of input vibrations. Mech. Syst. Signal Process. *125*, 215–228. https://doi.org/10.1016/j.ymssp.2018.05.062.

49. Malaji, P.V., and Ali, S.F. (2018). Analysis and experiment of magneto-mechanically coupled harvesters. Mech. Syst. Signal Process. *108*, 304–316. https://doi.org/10.1016/j.ymssp.2018.02.025.